Stability of ablation flows in inertial confinement fusion: non-modal effects

G Varillon, J.-M Clarisse, A. Couairon

Stability of ablation flows in inertial confinement fusion: non-modal effects

G. Varillon,[1,2] J.-M. Clarisse,[1] and A. Couairon[2]

[1] *CEA, DAM, DIF, F-91297 Arpajon, France*

[2] *CPHT, CNRS, Ecole Polytechnique, Institut Polytechnique de Paris, Route de Saclay, 91128 Palaiseau, France*[*]

(Dated: January 15, 2021)

Fast transient growth of hydrodynamic perturbations due to non-modal effects is shown to be possible in an ablation flow relevant to inertial confinement fusion (ICF). Likely to arise in capsule ablators with material inhomogeneities, such growths appear to be too fast to be detected by existing measurement techniques, cannot be predicted by any of the methods previously used for studying hydrodynamic instabilities in ICF, yet could cause early transitions to nonlinear regimes. These findings call for reconsidering the stability of ICF flows within the framework of non-modal stability theory.

I. INTRODUCTION

Inertial confinement fusion (ICF) has been proposed some 50 years ago as a viable means for harnessing thermonuclear fusion with the aim of producing energy. This scheme relies on the irradiation of spherical capsules of millimeter size, filled with thermonuclear fuel, at high energy fluxes capable of producing, over nanoseconds, a fuel compression of thousands of times solid density [1]. Such high compressions critically depend, however, on a mitigation of hydrodynamic instabilities during capsule implosion, since these may hamper the compression and heating of the fuel, possibly ruining the whole process. In particular, the subsonic heat-wave flow, or *ablation flow*, that results from the irradiation of the outer layer, the *ablator*, of a fusion capsule and drives its implosion, was right away considered as a dominant factor of hydrodynamic perturbation growth [2, 3]. Despite several decades of dedicated numerical simulations, experiments, theoretical works and improvements in the understanding, prediction and mitigation of capsule implosion perturbations, ICF is still in practice impeded by issues of hydrodynamic instability (e.g. Refs. 4–6).

The strongly compressible, nonuniform and unsteady nature of capsule implosions, besides the complexity of the high-temperature physics at stake, renders the study of their hydrodynamic stability especially arduous. Two types of approaches have then been pursued: (i) stability analyses using simplified physical modelings and (ii) computations of perturbation amplifications trying to be as realistic as possible. The framework of compressible inviscid fluid dynamics with nonlinear heat conduction has undoubtedly contributed to a better understanding of ablation flow instabilities (cf. the review of Ref. 7). Corresponding stability analyses have exclusively consisted in applying the method of normal modes, or *modal stability analysis*, for idealized reduced portions of the implosion flow (e.g. steady, quasi-isobaric, constantly accelerated, at times discontinuous, ablation flows) or more realistic, i.e. simulated, flows under the frozen-time assumption. Such analyses, since they focus on the least stable eigenmode of the flow, can only yield asymptotic stability results and are inevitably, given the implosion unsteadiness, of restricted validity in time and perturbation wavenumber ranges. Perturbation amplification computations belong to a different approach, sometimes called *amplification theory* (AT), which consists in computing responses of an arbitrary base flow, solution to an initial and boundary value problem (IBVP), to selected initial and/or boundary perturbations. Such computations are not sufficient by themselves for obtaining results of stability. Nevertheless, this approach has been widespread in ICF, especially using multi-dimensional hydrodynamics codes dedicated to ICF physics since the restrictive settings of theoretical models are thus avoided.

Yet another approach exists that has never been considered in ICF and which consists in applying methods of *non-modal stability theory* [8], the sole capable of giving stability results for unsteady flows, irrespective of time horizons. However, given available computational means, the task is daunting for a complete capsule implosion and it is therefore logical to start with a simpler flow. In the present work, we initiate this effort by performing a non-modal stability analysis of an unsteady ablation flow modeling the early stage of a capsule implosion.

Confidence in the ability of ICF hydrodynamics codes to reproduce instability dynamics has been progressively built through comparisons between AT computations and specifically designed experiments where a dominant, i.e. considered most detrimental, perturbation source is selected by carefully controlling experimental conditions (e.g. Refs. 9 and 10). However, AT computations, carried out with these very codes, still display unexplained discrepancies with ablation experiments on capsule ablators at standard specifications for fusion [11, 12]. The short history of ICF has shown that, among the many possible explanations, overlooking some perturbation sources or unappreciated effects is highest in the list [**?** , Sec. V]. For several decades, based on modal stability analyses, AT computations and dedicated experiments, roughness of the ablator surfaces was considered as the most detrimental perturbation source. Intensive efforts were spent on this issue, leading to surface finish requirements for

[*] gregoire.varillon@gmail.com

fusion. By then ablator material inhomogeneities were thought to play a minor role. This way of thinking was turned around by the experiments of Ref. [11]: ablator inhomogeneities could be in fact a major perturbation source [13]. In such experiments [11, 12], many perturbation sources are competing, without an artificial dominance of one on the others, and the characterization of their initial or temporal contributions is insufficient for setting up representative enough AT computations. Besides, it is known that perturbation eigenmodes that are stable according to modal stability theory can induce, through their interaction, perturbation transient growth [14]. Hence different perturbation sources—even though each of them, separately, are identified to be minor—could lead, upon proper combination, to perturbation amplification. Modal stability theory, by assuming that eigenmodes are orthogonal, ignores such interactions, or *non-modal effects*. In principle, AT computations could capture such growths provided that they are started from appropriate initial conditions. However, identifying systematically these most detrimental initial perturbations requires the use of methods that have never been considered in ICF. The alternative—a brute force use of AT computations for sampling the space of eligible initial conditions so as to, hopefully, find those leading to maximum amplification—is at best unrealistic. Therefore a genuine risk exists of missing the most detrimental perturbation sources due to a lack of a proper methodology.

Non-modal stability theory precisely furnishes such a methodology by fully exploiting the fact that the finite-time dynamics of a system is not only ruled by the eigenvalues of its evolution operator but also by this operator eigenmodes [15]. Elaborated over the last thirty years, this theory has been successful in elucidating some withstanding problems in hydrodynamic stability [8]. Until proven otherwise, non-modal effects and associated transient growths cannot be ruled out nor held as negligible in ICF ablation flows. By performing a linear non-modal analysis, local in space and time, we address the questions (i) of whether or not an ICF ablation wave may present non-modal effects, and (ii) of the associated mechanism(s) of transient growth.

In the rest of this article, we first present the chosen modelling and equations of motion for the base flow and linear perturbations (Sec. II). Necessary notions of non-modal analysis are then reviewed (Sec III A) and a local non-modal stability analysis of linear perturbations is performed, leading to initial conditions for maximal initial growth of perturbations (Sec. III B). Temporal responses of these maximal growth initial conditions are computed (Sec. III C) and the mechanisms underlying these transient growths are analysed (Sec. IV). The implications of the results in the context of ICF are discussed (Sec. V) and the main results are recalled (Sec. VI).

II. ABLATION FLOWS

The present stability analysis is conducted on a self-similar ablation flow in slab symmetry representative of the early stage of an ICF capsule implosion [16–19]. During this so-called *shock transit stage*, the leading shock front of the ablation wave has not yet reached the ablator inner surface and the capsule has not started its converging motion. Since the ablator is thin compared to the capsule radius, the approximation of slab symmetry is amply justified. The chosen self-similar flow presents the essential features of the subsonic heat wave that prevails within the capsule ablator during this stage of the implosion (compressibility, stratification, unsteadiness), including its whole structure (Fig. 1): (i) a leading shock front, (ii) a quasi-isentropic compression region, (iii) an ablation layer, and (iv) an expansion wave where heat conduction dominates ('conduction region').

A. Base flow

A dimensionless formulation of the equations of motion is retained so as to keep the flow description as general as possible [18, 20]. For one-dimensional motion along the x-axis of a Cartesian coordinate system (O, x, y, z), the equations of motion, written in the Lagrangian coordinate m where $\mathrm{d}m = \rho\,\mathrm{d}x$, come as

$$\begin{aligned} &\partial_t(1/\rho) - \partial_m v_x = 0,\\ &\partial_t v_x + \partial_m p = 0,\\ &\partial_t(\mathrm{C}_v T + v_x^2/2) + \partial_m(p v_x + \varphi_x) = 0, \end{aligned} \tag{1}$$

where ρ, v_x, p, T, φ_x denote, respectively, the fluid density, velocity, pressure, temperature and heat flux as functions of (m, t). The dimensionless equation of state for a polytropic gas,

$$p = \rho T, \quad \text{with} \quad \mathrm{C}_v = 1/(\gamma - 1),$$

γ being the fluid adiabatic exponent, and the heat-flux expression

$$\varphi_x = -\rho^{-\mu} T^{\nu}\, \rho\, \partial_m T, \quad \mu \geq 0, \quad \nu > 1,$$

supplement this system. For the choice $\gamma = 5/3$, $(\mu, \nu) = (2, 13/2)$, Eq. (1) describes the motion of a monatomic gas with the radiative conduction model of Kramers [21]. This modeling is an approximation for the ablation of a fusion capsule ablator by hohlraum x rays in current ICF laser facilities. This approximation is relevant to the ablator opaque portion which stays at temperatures below a few 10^6 Kelvin degrees and at thermodynamic equilibrium. Radiation diffusive effects then dominate those of thermal conduction and viscosity, and radiation pressure and energy are negligible in front of their material counterparts. If Eq. (1) cannot render non-gray irradiation effects, it contains the basic diffusion mechanism at stake, at the hydrodynamic scale, in this ablation process. Such a modeling of radiative ablation

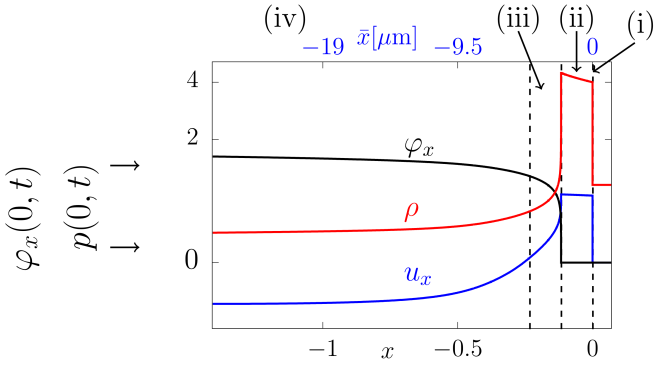

FIG. 1. Self-similar ablation-wave solution to Eq. (1) for $\gamma = 5/3$, $(\mu, \nu) = (2, 13/2)$ and boundary condition parameters $(\mathcal{B}_\phi, \mathcal{B}_p) = (0.8, 0.31)$. Dimensionless spatial profiles in the coordinate x at time $t_0 = 1$ of the fluid density ρ, longitudinal velocity v_x and heat flux φ_x. Correspondence with the actual physical extent of the wave, relative to the shock front, at the chosen reference time of a simulated capsule implosion is also indicated (top axis) (see App.).

compares favorably with any of the models previously used for investigating hydrodynamic stability of ablation flows and designing experiments (e.g. see Ref. 7 and references therein): it retains the same compressible inviscid fluid model for a polytropic gas with a nonlinear heat conductivity in powers of the density and temperature. However, none of the additional restrictive assumptions (e.g. flow steadiness, constant and uniform acceleration field, quasi-isobaric approximation, semi-infinite fluid domains) that are commonly used in these other stability studies of ablation flows, are invoked here.

Self-similar reductions of Eq. (1) occur when considering a semi-infinite slab ($m \geq 0$), initially such that $(\rho,\, v_x,\, T) = (\mathrm{const},\, 0,\, 0)$, is subject to boundary conditions, at the material surface $m = 0$, of the form

$$\varphi_x(0,t) = \mathcal{B}_\phi t^{3\alpha-3}, \quad p(0,t) = \mathcal{B}_p t^{2\alpha-2}, \quad \text{for } t \geq 0, \tag{2}$$

with $\alpha = (2\nu-1)/(2\nu-2)$: cf. Refs. [17–19]. Self-similar solutions to Eq. (1) with such initial and boundary conditions are presently computed by means of an adaptive multidomain Chebyshev method capable of a high accuracy description of the flow down to its finest scales [22]. This numerical method has been verified against results from a hydrocode simulation [18, Fig. 11] of an IBVP defined after Eqs. (1) and (2), and approximate analytical solutions [19, App. A].

For the present study, the base-flow solution $(\mathcal{B}_\phi, \mathcal{B}_p) = (0.8, 0.31)$ that has been retained (Fig. 1), is computed using 39 domains with 50 collocation points each. This solution has been chosen among a large set of self-similar ablation waves [19], on the basis of its hydrodynamic characteristic numbers which are typical of the early stage of a capsule implosion: subsonic ablation Mach number, high Froude number (> 80) at the ablation front, steep ablation front, and fast expansion flow with Chapman–Jouguet point (Fig. 1). In actual or simulated implosions, neither the radiative heat flux at the capsule external surface, nor the pressure exerted by the hohlraum filling gas, nor the capsule ablator opacity comply with the constraints required for self-similarity. Yet, spatial profiles of self-similar flow variables possess essential features that resemble those obtained in simulations of the shock transit stage of a realistic ICF capsule design: cf. Ref. 19, Fig. 2. In that respect, results obtained with the chosen self-similar ablation wave may be equally used in connection with a capsule ablation simulation.

B. Linear perturbations

The stability of flows ruled by Eq. (1) is studied using an Eulerian description of three-dimensional linear perturbations in the coordinate system (x, y, z). Once expressed with the Lagrangian coordinate m and Fourier transformed in the variables (y, z), the corresponding system of governing partial differential equations for the Fourier components of the linear perturbations of the density, $\widehat{\rho}$, longitudinal velocity, $\widehat{v}_x$, transverse divergence of the transverse velocity, $\widehat{d}_\perp$, and temperature, $\widehat{T}$, reads (cf. Ref. 20 and Eq. 4 in Ref. 23)

$$\begin{aligned}
&\partial_t\widehat{\rho} + \rho^2\,\partial_m\widehat{v}_x + \rho\,\partial_m v_x\,\widehat{\rho} + \rho\,\partial_m\rho\,\widehat{v}_x + \rho\,\widehat{d}_\perp = 0,\\
&\partial_t\widehat{v}_x + T\,\partial_m\widehat{\rho} + \rho\,\partial_m\widehat{T} - \rho^{-1}\,T\,\partial_m\rho\,\widehat{\rho}\\
&\qquad + \rho\,\partial_m v_x\,\widehat{v}_x + \partial_m\rho\,\widehat{T} = 0,\\
&\partial_t\widehat{d}_\perp - k_\perp^2\,\rho^{-1}\,T\,\widehat{\rho} - k_\perp^2\,\widehat{T} = 0,\\
&\partial_t\widehat{T} + \mathrm{C}_v^{-1}\,\rho\,\psi_{T'}\,\partial^2_{m^2}\widehat{T} + \mathrm{C}_v^{-1}\,\psi_\rho\,\partial_m\widehat{\rho} + \mathrm{C}_v^{-1}\,p\,\partial_m\widehat{v}_x\\
&\qquad + \mathrm{C}_v^{-1}\left[\partial_m(\rho\,\psi_{T'}) + \psi_T\right]\partial_m\widehat{T}\\
&\qquad + \mathrm{C}_v^{-1}\left[\partial_m\psi_\rho - \rho^{-1}\,\partial_m\psi\right]\widehat{\rho} + \rho\,\partial_m T\,\widehat{v}_x + \mathrm{C}_v^{-1}\,T\,\widehat{d}_\perp\\
&\qquad + \mathrm{C}_v^{-1}\left[\rho\,\partial_m v_x + \partial_m\psi_T - k_\perp^2\,\rho^{-1}\,\psi_{T'}\right]\widehat{T} = 0,
\end{aligned}$$

or in vector form

$$\partial_t\widehat{\mathbf{U}} = \mathcal{A}(m, t, \partial_m\cdot, k_\perp)\,\widehat{\mathbf{U}}, \quad \widehat{\mathbf{U}} = \left(\widehat{\rho}\;\widehat{v}_x\;\widehat{d}_\perp\;\widehat{T}\right)^\top, \tag{3}$$

with the convention

$$\psi(\rho, T, \partial_x T) \equiv -\rho^{-\mu}T^\nu\,\partial_x T = -\rho^{-\mu}T^\nu\rho\,\partial_m T,$$

and the notations ψ_ρ, ψ_T, $\psi_{T'}$ for the partial derivatives of the heat-flux function ψ with respect to the density, the temperature, and the temperature gradient. The perturbation evolution operator, $\mathcal{A}$, depends on space, time and the wavenumber $k_\perp = \sqrt{(k_y^2 + k_z^2)}$. When considering self-similar ablation waves solutions to Eqs. (1) and (2), boundary conditions for linear perturbations at the location, $m = m_{\mathrm{sf}}(t)$, of the leading shock-wave front are derived from the non-isothermal Rankine–Hugoniot relations for a perturbed shock front [20, App. B]. At the fluid external boundary, $m = 0$, perturbation boundary conditions correspond to the continuity of the pressure and heat flux supplemented by the kinematic boundary condition at this material surface (Eq. 5 of Ref. 23). For

the present study, zero perturbations for the state upstream to the shock front and for the incident heat flux and boundary pressure at the fluid external surface are retained.

Solutions to IBVPs based on Eq. (3) are computed, in space, using the same multidomain Chebyshev method as for Eq. (1) and, in time, with a three-step implicit-explicit Runge–Kutta scheme. Verification of this computational method has been performed in several instances by comparisons with exact perturbation solutions [24–27]. This method has also been previously used for computing linear perturbation responses in perturbed configurations of ablation waves relevant to ICF and corresponding to illumination asymmetries [17, 20, 28, 29] and to the ablative Richtmyer–Meshkov instability [29]. Corresponding results were analyzed to be in general agreement with previous models of perturbation evolution for laser imprinting [30, 31] and ablative Richtmyer–Meshkov instability [9, 32] with, however, distinctive differences emphasizing, in particular, the influence of the base-flow unsteadiness and stretching: see [17, 20, 29] for details and discussions.

III. LOCAL NON-MODAL STABILITY ANALYSIS

A. Necessary notions of non-modal analysis

Modal stability analysis infers the stability of a dynamical system, ruled by an equation like Eq. (3), from the sole basis of the least stable eigenvalue of its evolution operator, $\mathcal{A}$. This analysis is correct if the eigenmodes of $\mathcal{A}$ form an orthogonal set—equivalently, if the operator $\mathcal{A}$ is normal—and is otherwise only indicative of the long-time behavior of the system. For finite-time horizons, a non-normal operator $\mathcal{A}$ may induce transient growth of the system state variable through eigenmode interactions, even if the system is stable according to modal analysis [8, 15]. For a time-dependent evolution operator as in Eq. (3), the growth of the state variable $\widehat{\mathbf{U}}$ can be assessed at any given time t_* from the instantaneous growth rate of some chosen norm $\|\widehat{\mathbf{U}}\|$, namely [14]

$$\sigma(t_*) \equiv \left(\frac{1}{\|\widehat{\mathbf{U}}\|^2} \frac{\mathrm{d}\|\widehat{\mathbf{U}}\|^2}{\mathrm{d}t} \right)\bigg|_{t_*} = 2\,\mathrm{Re}\left(\frac{\langle \widehat{\mathbf{U}}, \mathcal{A}\,\widehat{\mathbf{U}} \rangle}{\langle \widehat{\mathbf{U}}, \widehat{\mathbf{U}} \rangle} \right)\bigg|_{t_*}, \quad (4)$$

where $\langle \cdot, \cdot \rangle$ denotes the scalar product associated to this norm. The global norm is here defined after the scalar product

$$\langle \widehat{\mathbf{U}}, \widehat{\mathbf{V}} \rangle = \frac{1}{2} \int_0^{m_{\mathrm{sf}}} \rho^{-1}\, \widehat{\mathbf{U}}^\dagger \widehat{\mathbf{V}}\, \mathrm{d}m,$$

where the upperscript † indicates the transconjugate. The ratio

$$\frac{\langle \widehat{\mathbf{U}}, \mathcal{A}\,\widehat{\mathbf{U}} \rangle}{\langle \widehat{\mathbf{U}}, \widehat{\mathbf{U}} \rangle}\bigg|_{t_*},$$

is known as the *numerical range* of the operator $\mathcal{A}|_{t_*}$ and defines a region of the complex plane which, in the case of an operator $\mathcal{A}$ of finite dimension, contains the spectrum of $\mathcal{A}|_{t_*}$. For a non-normal operator, as it is generally the case, the numerical range is larger than the convex hull of the spectrum. In the case of a normal operator, the two regions coincide [33]. In particular, this numerical range may protrude into the unstable half-plane ($\mathrm{Re} > 0$) even though the spectrum of $\mathcal{A}|_{t_*}$ may be confined to the stable half-plane ($\mathrm{Re} < 0$): cf. Fig. 2(c). In such a case *non-modal growth* occurs, i.e. an initial amplification—*transient growth*—of $\widehat{\mathbf{U}}$ may be observed, although all eigenvalues are stable according to modal stability analysis. The potential for such a transient growth is measured by means of the maximum of the instantaneous growth rate $\sigma(t_*)$ over all non-zero possible states, or *numerical abscissa* of $\mathcal{A}|_{t_*}$, say

$$\sigma_* \equiv \max_{\widehat{\mathbf{U}}} \sigma(t_*). \quad (5)$$

This numerical abscissa is given by the largest eigenvalue of the normal operator $(\mathcal{A} + \mathcal{A}^\dagger)|_{t_*}$ and is achieved when $\widehat{\mathbf{U}}$ is the principal eigenmode of this operator (cf. Ref. 14), thus defining the *optimal-growth initial condition* at time t_*, say $\widehat{\mathbf{U}}_*^{\mathrm{opt}}$. The situation of non-normal growth described above corresponds to the case $\max \mathrm{Re}(\Lambda) < 0 < \sigma_*$, where Λ denotes the eigenvalues of $\mathcal{A}|_{t_*}$. However non-modal effects are not restricted to this specific configuration. Indeed, when $0 < \max \mathrm{Re}(\Lambda) < \sigma_*$ [Fig. 2(b)], the system is unstable at all time horizons but may display a transient growth that is faster than the exponential growth of the least stable eigenmode. For $\max \mathrm{Re}(\Lambda) < \sigma_* \leq 0$ [Fig. 2(a)], the system is stable, here again at all time horizons, but with an eventual transient decay that is slower than the exponential decay of the least stable eigenmode.

B. Maximal initial growth rate

The possibility of perturbation short-time growth for the self-similar ablation wave of Fig. 1 is investigated by means of a local analysis, in time and space, of Eq. (3). In effect, for some reference time $t_0 > 0$ and at any location $x_\circ = x(m_\circ, t_0)$ within the wave extent, we consider perturbations of longitudinal characteristic lengths that are shorter than the smallest local gradient length of the flow, say $l_\nabla(x_\circ)$. Under this assumption of a weakly stratified flow the operator $\mathcal{A}|_{t_0}$ may be held as uniform over a neighborhood of $x_\circ$, reducing the analysis of Eq. (3) to that of the m-Fourier transform of $\mathcal{A}|_{t_0}$, say $\mathcal{A}_0$, under the condition $\varkappa_x(x_\circ) \equiv \rho(x_\circ)\, k_m\, l_\nabla(x_\circ) \gg 1$ bearing on the longitudinal wavenumber k_m. Perturbation transient growth is then assessed at $t_* = t_0$ by computing the maximum instantaneous growth rate $\sigma_0(k_m, k_\perp, m_\circ)$, which, in this configuration of longitudinal Fourier trans-

(a) modal stability: slower transient decay

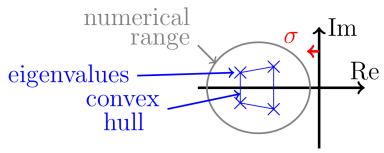

(b) modal instability: faster transient growth

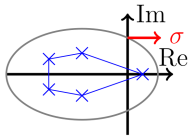

(c) modal stability: **transient growth**

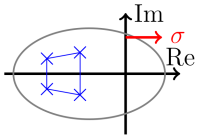

FIG. 2. Schematic layouts in the complex plane of eigenvalues and numerical ranges corresponding to: (a) modal stability with slower non-modal transient decay, (b) modal instability with faster non-modal transient growth, and (c) modal stability with non-modal transient growth.

form amounts to

$$\sigma_0(k_m, k_\perp) \equiv \max_{\widetilde{\mathbf{U}}_*} \left(\frac{1}{\|\widetilde{\mathbf{U}}_*\|^2} \frac{\mathrm{d}\|\widetilde{\mathbf{U}}_*\|^2}{\mathrm{d}t} \right)\Big|_{t_0}, \qquad (6)$$

where $\widetilde{\mathbf{U}}_*$ stands for the m-Fourier component of the restriction of $\widehat{\mathbf{U}}$ to a neighborhood of m_*. Such computations [34] are carried out for $m_\circ$ covering the whole extent of the ablation wave, for ranges of k_m such that $\varkappa_x(x_\circ) \geq 10$, and for different values of $k_\perp$. Maps of σ_0 as a function of the flow location $x_\circ$ and of the normalized longitudinal wavenumber $\varkappa_x$ are thus obtained (Fig. 3). Regions of non-modal growth, i.e. regions of modal stability but with positive σ_0 [configuration of Fig. 2(c)], are identified (colored areas in Fig. 3a) and distinguished from regions of modal instability [configuration of Fig. 2(b)] (black areas). Sizable portions of the conduction region ($-1.15 \lessapprox x \lessapprox -0.12$), the ablation layer ($x \approx -0.12$), for extended ranges of $\varkappa_x$, and the compression region ($-0.12 < x < 0$), for restricted $\varkappa_x$, are prone to non-modal growth. In regions of modal instability [black areas in Fig. 3(a)], the numerical range is larger than $\max \mathrm{Re}(\Lambda)$ (Fig. 3b), indicating a configuration of faster transient growth [configuration of Fig. 2(b)]. These observations depict a situation where the local short-term dynamics of flow fluctuations are determined by non-modal effects, implying that modal stability analysis is nowhere suitable for their predictions and that perturbation transient amplifications have to be taken into account and searched for. In short, for all the perturbation wavelengths that have been tested, the perturbation evolution operator for an ablation wave driven by nonlinear heat conduction is non normal.

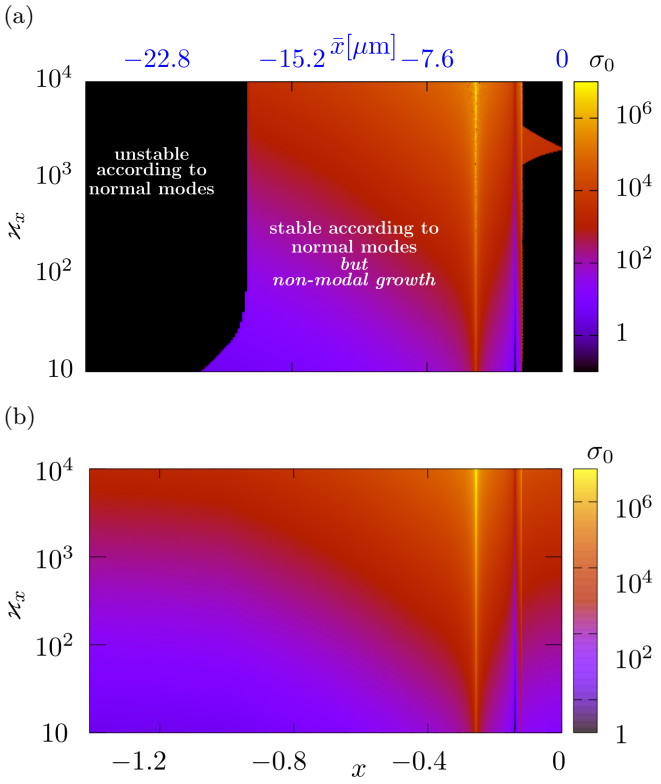

FIG. 3. Intensity map, in the plane $(x, \varkappa_x)$, of $\log \sigma_0$, $\sigma_0 > 0$, obtained from Eq. (5) for $k_\perp = 1.2$: (a) regions of non-modal growth but modal stability (color) and regions of modal instability (black), and (b) $\sigma_0 - \max \mathrm{Re}(\Lambda)$ everywhere. Same horizontal axis conventions as in Fig. 1.

C. Responses to optimal-growth initial perturbations

The actual occurrence of non-modal growth is confirmed by means of AT computations of $\widehat{\mathbf{U}}$ by solving Eq. (3) for $t \geq t_0 = 1$ with the aforementioned boundary conditions at the external surface and shock front (Sec. II B). Initial conditions, inferred from the above non-modal stability analysis, are defined so as to comply with the assumption of a weakly stratified flow. For a given longitudinal wavenumber k_m, the solution is reconstructed from $\widetilde{\mathbf{U}}_0^{\mathrm{opt}}$ (see Sec. III A) as

$$\widehat{\mathbf{U}}(m, t_0, k_\perp) = w(m, k_m)\, \mathrm{Re}\big(\widetilde{\mathbf{U}}_0^{\mathrm{opt}}(m_\circ, k_m, k_\perp)\, e^{ik_m m}\big), \qquad (7)$$

where w is a sufficiently smooth mask function, non-zero over a limited domain centered on $m = m_\circ$. The comparison of the measured initial growth rate σ_{AT} of the

intial condition (7) with the numerical abscissa, or *optimal growth rate*, σ_0 assesses the relevance of the local non-modal analysis. If $\sigma_{\rm AT}$ and σ_0 are close, then the dominant mechanisms are captured by the local analysis. Otherwise the local analysis misses some major features.

Results obtained at a midpoint location within the compression region for normalized wavenumbers $\varkappa_x$, $\varkappa_\perp = k_\perp\, l_\nabla(x_\circ)$ for which the method of normal mode predicts stability, are exemplified in Table I(a) and illustrated in Figs. 4(a), 5 and IV(a). Additional results at a location immediately upstream to the ablation layer are illustrated in Figs. 4(b) and IV(b). Growth rates $\sigma_{\rm AT}$, extracted from AT computations with initial conditions (7), are in good agreement with the values of $\sigma_0(k_m, k_\perp)$ given by Eq. (5). This agreement and growth times, $\sigma_{\rm AT}^{-1}$, much smaller than the base-flow characteristic time, here $t \approx 1$, validate the local analysis leading to Eq. (5). Through these simulations, initial transient growth is verified at flow locations where modal stability analysis predicts decaying perturbations, thus substantiating the reality of local non-modal effects in a typical ablation flow. The

TABLE I. (a) Characteristic growth times: σ_0^{-1} 'predicted' via Eq. (5) for the flow location $x_\circ = -0.06$, and $\sigma_{\rm AT}^{-1}$ extracted from AT computations. (b) Corresponding values obtained for the chosen reference time of a simulated capsule implosion(see App.) at the equivalent location, 1.1 μm downstream to the shock front.

(a)

$(\varkappa_x, \varkappa_\perp)$	(1758., 1.40)	(1758., 5.26)	(1758., 131.5)
$\sigma_0^{-1}\,(10^{-5})$	15.7	15.7	8.06
$\sigma_{\rm AT}^{-1}\,(10^{-5})$	15.2	15.2	7.87

(b)

$(\bar\lambda_x, \bar\lambda_\perp)\,(\mu{\rm m})$	(0.080, 100.)	(0.080, 26.6)	(0.080, 1.06)
$\bar\sigma_{\rm AT}^{-1}\,({\rm ps})$	0.22	0.22	0.11

corresponding transient growths, with significant amplifications of the perturbation norm (event A, Fig. 4a), result from the constructive interaction between the localized entropy and acoustic waves that dominate the optimal-growth initial conditions (7) [event A, Figs. 5(a–d)]. The ensuing perturbation dynamics proceed from further mutual interactions of these waves [events A and C, Figs. 4a and 5(a-c)], their propagation [Figs. 5(b,c,d)], and interactions with the ablation layer [event B, Figs. 4a and 5(a,b,d)] and shock front [event D, Figs. 4a and 5(a,b)].

Hydrodynamic disturbances are classically detected in ICF through measurements of longitudinal optical depth perturbation [10], presently amounting to

$$\widehat{\rm OD} = \int_0^{m_{\rm sf}} \rho^{-1}\,(\kappa_\rho\,\widehat\rho + \kappa_T\,\widehat T)\,{\rm d}m + [\partial_x\kappa\,\widehat x]_{\rm es}^{\rm sf}$$

where $\kappa = 4\,\rho^\mu T^{3-\nu}$ is the fluid opacity [35], and $\widehat x_{\rm es|sf}$, the deformation of the external surface|shock front. The perturbation of the longitudinal optical depth is notably

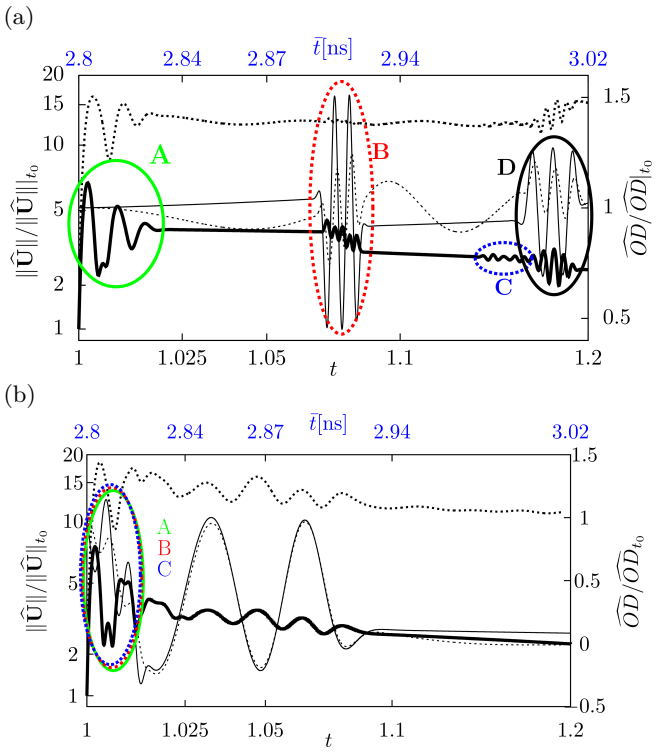

FIG. 4. Amplification of the perturbation norm, $\|\widehat{\mathbf U}\|/\|\widehat{\mathbf U}\|_{t_0}$, (thick lines—left axis) and of the optical depth perturbation, $\widehat{\rm OD}/\widehat{\rm OD}|_{t_0}$ (thin lines—right axis), for initial conditions Eq. (7) at (a) a midpoint location within the compression region, $x_\circ = -0.06$, and (b) a location immediately upstream to the ablation layer, $x_\circ = -0.11$, with $\varkappa_x = 1758.$, $\varkappa_\perp = 1.40$ (solid) or $\varkappa_\perp = 131.5$ (dash). Remarkable events in the evolution of $\|\widehat{\mathbf U}\|$ are identified by letters A to D.

insensitive to the transient growth, varying only when waves interact with the ablation layer and shock front (events B and D, Fig. 4a).

IV. TRANSIENT GROWTH MECHANISM: CONSTRUCTIVE INTERACTION OF COMPRESSIBLE WAVES

The dynamics of perturbations in the flow compression region, i.e. between the shock front and the ablation layer, during the shock transit stage of a capsule implosion deserve special attention. These dynamics are especially important for the outcome of the implosion since they set the initial conditions for the subsequent acceleration stage during which major perturbation amplification occurs due to the ablative Rayleigh–Taylor instability. The computations of perturbation evolutions, started from the optimal-growth initial conditions of Eq. (7) at locations within the compression region, show that the fastest transient growth comes from the constructive interaction between the different fundamental waves—or Kovásznay modes [36]—that constitute these initial per-

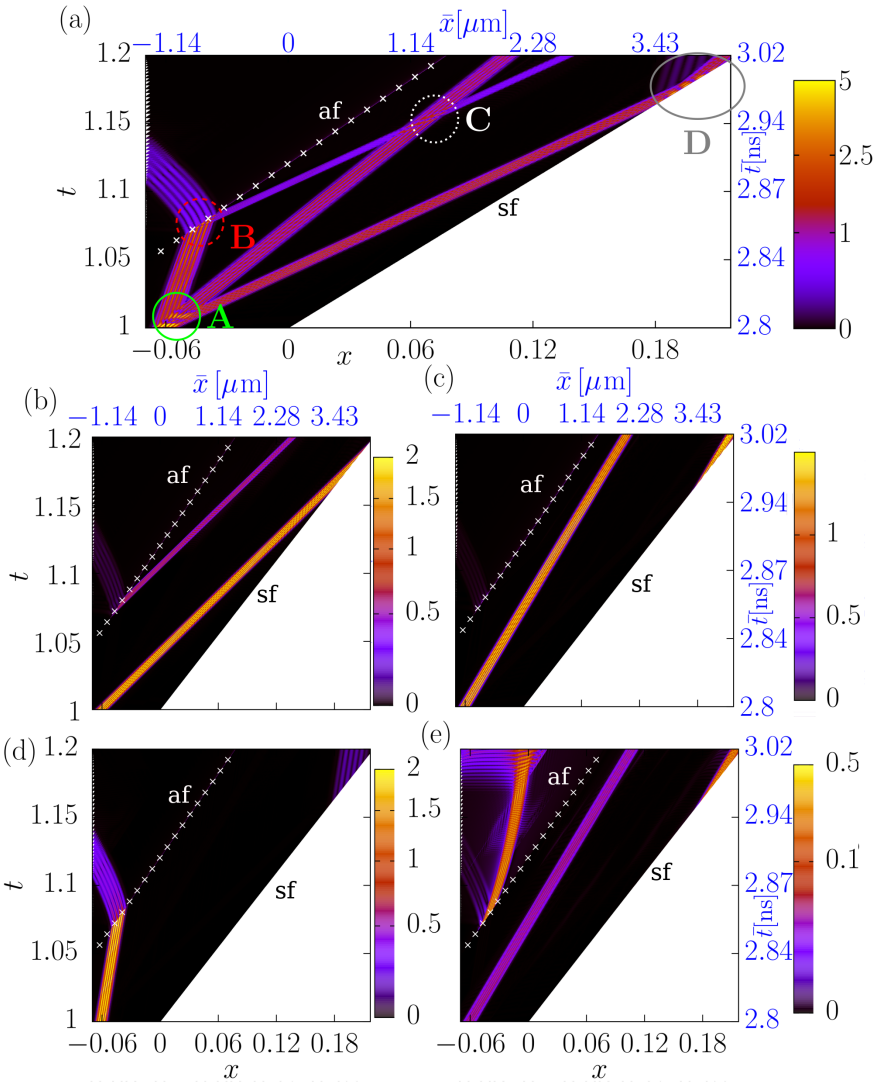

FIG. 5. Evolution of $\widehat{\mathbf{U}}$ in the compression region for initial conditions Eq. (7) at $x_\circ = -0.06$, in the case $(\varkappa_x, \varkappa_\perp) = (1758, 1.40)$. Same conventions as in Fig. 1 with shock (sf) and ablation (af) front trajectories. (a) Local Euclidean norm. Components (absolute value) in longitudinal pseudo-characteristic variables [23]: (b) forward and (d) backward acoustic waves, (c) entropy waves. (e) Transverse potential vorticity. Labelled circles in (a) relate to the events identified in Fig. 4a.

turbations (see Fig. 5) for $t \simeq 1$). For the sample of transverse wavelengths considered (Table I), these fundamental waves are dominantly of the acoustic and entropy types, the initial vorticity waves being of negligible contributions. This mechanism of wave interaction is intrinsic to compressible fluid motion and is expected to occur in the compression regions of actual ablation flows since in such regions effects of advection prevail over those of heat transfer.

Corresponding dimensional data obtained in connection with a simulation of a chosen ICF capsule implosion (see App.) are given in Table I(b), on upper axes of Figs. 4 and IV, and upper and right axes of Fig. 5. The associated figures are indicative of characteristic lengths of perturbations that are susceptible to yield transient growth. The perturbations presently identified are in the tens of nanometers in the longitudinal (or radial) direction and within the range 1–100 microns in the transverse (or azimuthal) direction, corresponding for the chosen capsule to Legendre modes ranging from 60 to 6000. These lengths fall within the characteristic sizes of known bulk inhomogeneities of currently used ablator materials [12].

In the flow compression region during the shock transit stage, these materials are in a complex liquid state (densities of several $\mathrm{g\,cm^{-3}}$, temperatures around 1 eV), partially dissociated and ionized, which is far from being known with sufficient details and is still the object of ongoing studies. The characteristic growth times $\sigma_{\mathrm{AT}}^{-1}$ of the identified transient growths are especially small: tenths of a picosecond [Table 1(b)]. For CH plastic ablators, such times are an order of magnitude larger than the

acoustic transit time between atoms and thus compatible with the assumption of local thermodynamic equilibrium for translation motions. Non-equilibrium effects associated to rotation and vibration motions cannot be ruled out but their assessment would require a more detailed knowledge of these ablator materials under these liquid state conditions. Effects of thermal conduction and of viscosity on this transient growth mechanism would also need to be assessed at the perturbation scales of tens of nanometers which are involved [Table 1(b)]. But here again adequate data and modelings relevant to these specific liquid states are currently unsufficient for doing so.

Past the initial growth, the contructive interaction of acoustic and entropy waves associated to the present transient growth leads to perturbation amplifications in the range 5–20 in a few picoseconds (Fig. 4). These amplifications, as the instantaneous growth rates, are enhanced by a reduction of the transverse wavelength: compare the perturbation norm responses, $\|\widehat{\mathbf{U}}\|/\|\widehat{\mathbf{U}}\|\|_{t_0}$, for the two wavenumbers $\varkappa_\perp = 1.40$ ($\lambda_\perp \approx 100\,\mu$m) and $\varkappa_\perp = 131.5$ ($\lambda_\perp \approx 1\,\mu$m) in Fig. 3. The residual amplifications, once the initial wave interactions have ended [i.e. after event A in Figs. 4 and 5(a)], slowly decrease over tenths of nanoseconds while remaining at significant levels. Such evolutions correspond to the advection, or propagation, (see Fig. 4) of the three kinds of waves (i.e. entropy waves plus forward and backward propagating acoustic waves) that are present in the initial perturbations, and to their subsequent interactions with either the ablation layer (event B) or the shock front (event D). All of these processes and trends are reproduced for other locations of the optimal-growth initial conditions Eq. (7), with a systematic enhancement of amplifications when the zone of transient growth, or *transient-growth spot*, is close and upstream to the ablation layer, as illustrated in Fig. 4(b) by comparison with 4(a). This increased influence of a transient-growth spot located close to the ablation layer is also obvious from the dynamics of the ablation front deformations (Fig. IV). ht!]

(a)

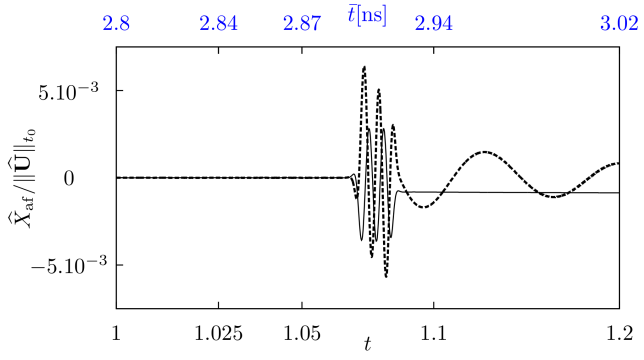

(b)

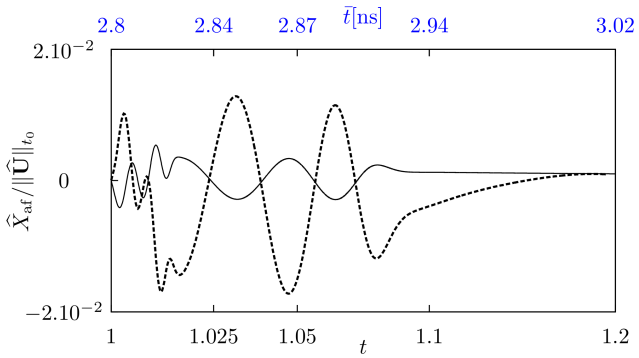

Time evolutions of the ablation front deformation, normalized by $\|\widehat{\mathbf{U}}\|\|_{t_0}$, for initial conditions Eq. 4 at (a) a midpoint location within the compression region, $x_\circ = -0.06$, and (b) a location immediately upstream to the ablation layer, $x_\circ = -0.11$, with $\varkappa_x = 1758.$, $\varkappa_\perp = 1.40$ (solid) or $\varkappa_\perp = 131.5$ (dash).

V. DISCUSSION

This analysis of the consequences of constructive interactions of compressible waves on the compression region and ablation layer of an ablation flow presently involves isolated transient-growth spots that are of limited spatial extents (in effect, five longitudinal wavelengths). The conditions for the occurrence of such constructive interactions—the presence of acoustic and entropy plane waves of identical, or proportional, longitudinal wavelengths—are likely to be met in ablators presenting bulk material inhomogeneities. In such configurations, the leading shock front of the ablation wave, encountering these inhomogeneities, emits backward propagating acoustic waves and leaves entropy/vorticity waves in the flow compression region downstream (cf. Ref. [**?**]). These waves will trigger emission, from the ablation layer, of forward propagating acoustic waves—as in the case of event B in Fig. 4(a)—which will in turn interact with upstream acoustic and entropy waves, at times constructively. For randomly distributed material inhomogeneities, constructive interactions will occur repeatedly giving birth to distributions of transient-growth spots within the compressed portion of the ablator. The repetitive encounters of these spots with the ablation layer could result in an enhanced level of perturbations, including ablative Rayleigh–Taylor modes, at the onset of the acceleration phase of a capsule implosion. Besides, this process could foster a build up of perturbations over a wide range of characteristic lengths and over times shorter than the duration of the shock transit phase, leading possibly to local transitions to nonlinear regimes. Assessing the possibility of such mechanisms and their consequences for an ICF capsule ablation would require flow simulations not only at extremely fine spatial resolutions, which so far have been undertaken only once [5], their results showing enhanced shock-front perturbations, but

also, given the nature of the transient-growth mechanism, capable of a high fidelity rendering of acoustic phenomena at very disparate scales—something for which ICF hydrodynamics codes are not particularly suited.

The insensitivity of the longitudinal optical depth to transient growth and the growth time scales (Fig. 4a), way below current experimental measurement capabilities, make the experimental detection of the above fast amplification dynamics most unlikely in practice. Ablator materials with bulk inhomogeneities, such as those used in the experiments of Ref. [12], are likely to induce constructive interactions of fluid waves since such inhomogeneities trigger emissions by the shock front (ablation layer) of acoustic and entropy (respectively, acoustic) fluctuations. High density carbon or beryllium materials for ablators can hardly be processed so as to impose controlled bulk inhomogeneities, similarly to what has been done for oxygen concentration in CH plastic ablators. Therefore the detection of transient growth events mainly relies on improved diagnostics. Firstly, current diagnostics do not have sufficient temporal resolutions to capture sub-nanosecond growth phenomena. Secondly, optical depth measurements in the longitudinal direction are blind to compressible perturbation modes, as shown on Figs. 4a and 4b. Optical depth measurements in a direction transverse to the flow could yield some information about the dynamics and spatial structures of perturbations in the flow compression region, but under conditions of sufficiently high temporal and spatial resolutions that so far are not available.

Simulations with surface roughness alone could not explain the levels of shock-front non-uniformities that were observed in these experiments. However the leading mechanisms responsible for such perturbation levels are still uncertain and cannot be unraveled on the sole basis of available experimental and simulation data. The present transient growth mechanism is potentially one of them, contributing to perturbation amplification in the compression region and the ablation layer, and thus to an enhanced seeding of ablative Rayleigh–Taylor modes for the subsequent acceleration stage of a capsule implosion. Assessing the importance of this mechanism in capsule implosions requires therefore experimental diagnostics and/or detailed analyses of high-fidelity simulations that have yet to come.

VI. CONCLUSION

The present work brings the first evidences of non-modal effects in the stability of an ablation flow related to ICF. In effect, local transient growth of perturbations may occur in flow regions that are stable according to the classical method of normal modes. The identified mechanism of transient growth is intrinsic to compressible fluid motion and thus generic to any ICF ablation flow. This mechanism puts forth the possibility, in an ablator with material inhomogeneities, of fast perturbation amplifications, not directly detectable by existing experimental diagnostics but contributing to perturbation enhancement. Such amplifications, compatible with trends observed in inhomogeneous ablator experiments and simulations, could induce transitions to perturbation nonlinear regimes earlier than foreseen by modal stability analysis. Global non-modal stability analyses and high-fidelity simulations would at least be needed to investigate such a possibility, which cannot be neglected until proven otherwise. More generally these findings call for applying methods of non-modal stability theory to ICF implosions so as to establish on firmer grounds their predictions, thus reducing uncertainties thereof.

Appendix: Connection with a capsule implosion simulation

Considering a particular ICF capsule design (here that given in Ref. 37, Fig. 1) and its implosion simulation with an ICF hydrocode (code FCI2, cf. Ref. 38), time and length scales may be defined respectively from the duration of the ablation flow regime within the period of the shock transit stage, and the distance travelled by the leading shock front during this period. The starting time of this ablation regime is established as being one of the earliest times for which, in the simulation, an ablation wave structure with a non-vanishing extent of its shock-compressed region is clearly identified within the ablator, presently $\bar{t}_0 = 2.8\,\mathrm{ns}$. This starting time is associated to the reference time of the self-similar ablation wave which may be set arbitrarily to be $t_0 = 1$. The final time of the ablation regime, in the simulation, is taken to be the time of the leading shock-front breakout at the ablator inner surface, here $\bar{t}_1 = 12.9\,\mathrm{ns}$. Over the flow period thus defined, a linear perturbation initiated at the ablation front may propagate as a forward acoustic wave towards the shock front then back to the ablation front as an advected entropy wave [23], the whole being repeated a limited number of times. This finite sequence of propagation-then-advection of perturbations between the ablation and shock fronts is a key mechanism of perturbation dynamics during the shock transit stage: e.g. see Refs. [9, 30]. Seeking to reproduce the same wave sequence in the present self-similar flow is therefore desirable, and presently sets a lower bound on the maximum time horizon for this flow, here $t_1 = 8$. The correspondence of flow durations and shock travelled distances between the simulated flow and the self-similar solution defines then time and length scales for the latter, in effect $t_\star = 1.44\,\mathrm{ns}$ and $l_\star = 19.04\,\mu\mathrm{m}$.

[1] S. Atzeni and J. Meyer-ter-Vehn. *The physics of inertial fusion*. Oxford University Press, Oxford, U.K., 2004.

[2] S. E. Bodner. Rayleigh–Taylor instability and laser-pellet fusion. *Phys. Rev. Lett.*, 33(13):761–764, 1974.

[3] J. D. Lindl and W. C. Mead. Two-dimensional simulation of fluid instability in laser-fusion pellets. *Phys. Rev. Lett.*, 34(20):1273–1276, 1975.

[4] J. Lindl, O. Landen, J. Edwards, E. Moses, and NIC Team. Review of the National Ignition Campaign 2009-2012. *Phys. Plasmas*, 21:020501, 2014.

[5] Brian M. Haines, R. E. Olson, W. Sweet, S. A. Yi, A. B. Zylstra, P. A. Bradley, F. Elsner, H. Huang, R. Jimenez, J. L. Kline, C. Kong, G. A. Kyrala, R. J. Leeper, R. Paguio, S. Pajoom, R. R. Peterson, M. Ratledge, and N. Rice. Robustness to hydrodynamic instabilities in indirectly driven layered capsule implosions. *Physics of Plasmas*, 26(1):012707, 2019.

[6] D. S. Clark, C. R. Weber, J. L. Milovich, A. E. Pak, D. T. Casey, B. A. Hammel, D. D. Ho, O. S. Jones, J. M. Koning, A. L. Kritcher, M. M. Marinak, L. P. Masse, D. H. Munro, M. V. Patel, P. K. Patel, H. F. Robey, C. R. Schroeder, S. M. Sepke, and M. J. Edwards. Three-dimensional modeling and hydrodynamic scaling of national ignition facility implosions. *Physics of Plasmas*, 26(5):050601, 2019.

[7] V. Bychkov, M. Modestov, and C. K. Law. Combustion phenomena in modern physics: I. Inertial confinement fusion. *Prog. Energy Combust. Sci.*, 47:32–59, 2015.

[8] P. J. Schmid. Nonmodal stability theory. *Annu. Rev. Fluid Mech.*, 39:129–162, 2007.

[9] Y. Aglitskiy et al. Basic hyrdodynamics of Richtmyer–Meshkov-type growth and oscillations in the inertial confinement fusion-relevant conditions. *Phil. Trans. R. Soc. A*, 368:1739–1768, 2010.

[10] K. S. Raman, V. A. Smalyuk, D. T. Casey, S. W. Haan, D. E. Hoover, O. A. Hurricane, J. J. Kroll, A. Nikroo, J. L. Peterson, B. A. Remington, H. F. Robey, D. S. Clark, B. A. Hammel, O. L. Landen, M. M. Marinak, D. H. Munro, K. J. Peterson, and J. Salmonson. An in-flight radiography platform to measure hydrodynamic instability growth in inertial confinement fusion capsules at the National Ignition Facility. *Phys. Plasmas*, 21:072710, 2014.

[11] V. A. Smalyuk et al. Hydrodynamic instability growth of three-dimensional, "native-roughness" modulations in x-ray driven, spherical implosions at the National Ignition Facility. *Phys. Plasmas*, 22:072704, 2015.

[12] S. J. Ali et al. Probing the seeding of hydrodynamic instabilities from nonuniformities in ablator materials using 2D velocimetry. 25(9):092708, 2018.

[13] S. W. Haan, H. Huang, M. A. Johnson, M. Stadermann, S. Baxamusa, S. Bhandarkar, D. S. Clark, V. Smalyuk, and H. F. Robey. Instability growth seeded by oxygen in CH shells on the National Ignition Facility. *Phys. Plasmas*, 22(3):032708, 2015.

[14] P. J. Schmid and D. S. Henningson. *Stability and transition in shear flows*. Springer, 2001.

[15] L. N. Trefethen et al. Hydrodynamic stability without eigenvalues. *Science*, 261:578–584, 1993.

[16] R. Marshak. Effect of radiation on shock wave behavior. *Phys. Fluids*, 1(1):24–29, 1958.

[17] F. Abéguilé, C. Boudesocque-Dubois, J.-M. Clarisse, S. Gauthier, and Y. Saillard. Linear perturbation amplification in self-similar ablation flows of inertial confinement fusion. *Phys. Rev. Lett.*, 97:035002, 2006.

[18] C. Boudesocque-Dubois, S. Gauthier, and J.-M. Clarisse. Self-similar solutions of unsteady ablation flows in inertial confinement fusion. *J. Fluid Mech.*, 603:151–178, 2008.

[19] J.-M. Clarisse, J.-L. Pfister, S. Gauthier, and C. Boudesocque-Dubois. A hydrodynamic analysis of self-similar radiative ablation flows. *J. Fluid Mech.*, 848:219–255, 2018.

[20] J.-M. Clarisse, C. Boudesocque-Dubois, and S. Gauthier. Linear perturbation response of self-similar ablative flows relevant to inertial confinement fusion. *J. Fluid Mech.*, 609:1–48, 2008.

[21] Ya. B. Zel'dovich and Yu. P. Raizer. *Physics of shock waves and high-temperature hydrodynamic phenomena*. Academic Press, New-York, 1967.

[22] C. Boudesocque-Dubois, V. Lombard, S. Gauthier, and J.-M. Clarisse. An adaptive multidomain Chebyshev method for nonlinear eigenvalue problems: Application to self-similar solutions of gas dynamics equations with nonlinear heat conduction. *J. Comput. Phys.*, 235:723–741, 2013.

[23] G. Varillon, J.-M. Clarisse, and A. Couairon. Investigation of supersonic heat-conductivity hyperbolic waves in radiative ablation flows. *Phys. Rev. E*, 101:043215, Apr 2020.

[24] C. Boudesocque-Dubois, J.-M. Clarisse, and S. Gauthier. A spectral Chebyshev method for linear stability analysis of one-dimensional exact solutions of gas dynamics. *J. Comput. Phys.*, 184:592–618, 2003.

[25] F. Abéguilé. *Etude de l'instabilité hydrodynamique d'écoulements autosemblables d'ablation*. Thèse de doctorat, Université de Paris 6, 2004.

[26] S. Gauthier, B. Le Creurer, F. Abéguilé, C. Boudesocque-Dubois, and J.-M. Clarisse. A self-adaptive domain decomposition method with Chebyshev method. *Int. J. Pure Appl. Math.*, 24:553–577, 2005.

[27] G. Varillon. *Nonmodal hydrodynamic stability analysis of ablation flows relative to inertial confinement fusion*. Thèse de doctorat, Université Paris-Saclay, École polytechnique, 2019.

[28] V. Lombard, S. Gauthier, J.-M. Clarisse, and C. Boudesocque-Dubois. Kovásznay modes in stability of self-similar ablation flows of ICF. *Europhys. Lett.*, 84:25001, 2008.

[29] J.-M. Clarisse, S. Gauthier, L. Dastugue, A. Vallet, and N. Schneider. Transient effects in unstable ablation fronts and mixing layers in HEDP. *Phys. Scr.*, 91:074005, 2016.

[30] V. N. Goncharov, S. Skupsky, T. R. Boehly, J. P. Knauer, P. McKenty, V. A. Smalyuk, R. P. Town, O. V. Gotchev, R. Betti, and D. D. Meyerhofer. A model of laser imprinting. *Phys. Plasmas*, 7(5):2062–2068, 2000.

[31] V. N. Goncharov, O. V. Gotchev, E. Vianello, T. R. Boehly, J. P. Knauer, P. W. McKenty, P. B. Radha, S. P. Regan, T. C. Sangster, S. Skupsky, V. A. Smalyuk, R. Betti, R. L. McCrory, D. D. Meyerhofer, and C. Cherfils-Clérouin. Early stage of implosion in inertial confinement fusion: Shock timing and perturbation

evolution. *Phys. Plasmas*, 13:012702, 2006.

[32] V. N. Goncharov. Theory of the ablative Richtmyer-Meshkov instability. *Phys. Rev. Lett.*, 82(10):2091–2094, 1999.

[33] R.A. Horn and C. R. Johnson. *Matrix Analysis*. Cambridge University Press, 1990.

[34] Carl C. Cowen and Elad Harel. An effective algorithm for calculating the numerical range, 9 1995.

[35] D. Mihalas and B. W. Mihalas. *Foundations of radiation hydrodynamics*. Oxford University Press, Oxford, 1984.

[36] L. S. G. Kovásznay. Turbulence in supersonic flow. *J. Aeronautic. Sci.*, 20(10):657–674, 1953.

[37] Y. Saillard. Hydrodynamique de l'implosion d'une cible FCI. *C. R. Acad. Sc. Paris*, t. 1, Série IV:705–718, 2000.

[38] E. Buresi, J. Coutant, R. Dautray, M. Decroisette, B. Duborgel, P. Guillaneux, J. Launspach, P. Nelson, C. Patou, J.-M. Reisse, and J.-P. Watteau. Laser program development at CEL-V: overview of recent experimental results. *Laser Part. Beams*, 4:531, 1986.